

## Upper Bound Limit Analysis of Anisotropic Soils

Chunguang Li<sup>1, \*</sup>, Cuihua Li<sup>2</sup> and Cong Sun<sup>3</sup>

**Abstract:** In this paper, a novel discretization method in  $\sigma$ - $\tau$  space is developed to calculate the upper bound limit loads and failure modes of anisotropic Mohr-Coulomb materials. To achieve this objective, the Mohr-Coulomb yield criterion is linearized in  $\sigma$ - $\tau$  space, which allows for upper bound solution of soils whose cohesion and friction coefficient varying with direction. The finite element upper limit analysis formulation using the modified anisotropic yield criterion is then developed. Several examples are given to illustrate the capability and effectiveness of the proposed numerical procedure for computing rigorous upper bounds for anisotropic soils.

**Keywords:** Anisotropy, limit analysis, upper bound, finite element.

### 1 Introduction

Natural soils and sedimentary rocks are typically formed by deposition and progressive consolidation during formation, giving rise to anisotropic behavior of the mechanical properties. In many cases the anisotropy will play a significant role in the stress distribution and the location of the failure surface of anisotropic structures.

More and more frequently in the last decades, a number of researchers focused on the studying of anisotropy role in geotechnical stability problems with limit analysis methods and limit equilibrium methods [Lo (1966); Chen, Snitbhan and Fang (1975); Reinicke and Ralston (1977); Yu and Sloan (1994); Al-Karni and Al-Shamrani (2000); Nian, Chen, Luan et al. (2008); Han, Chen, Xia et al. (2014)]. One of the early attempts at studying the anisotropic slope stability was made by Lo [Lo (1965)], he established an empirical anisotropic strength criterion based on the unconfined compressive strengths for soil specimens sampled at different orientations and found that the effect of anisotropy is more predominant in flatter slope than steeper one. Yu et al. [Yu and Sloan (1994)] proposed a finite element formulation of the bound theorems which generalized the conventional isotropic Mohr-Coulomb yield criterion to include the effect of variation of cohesion with direction in cohesive-frictional

---

<sup>1</sup> State Key Laboratory of Geomechanics and Geotechnical Engineering, Institute of Rock and Soil Mechanics, Chinese Academy of Sciences, Wuhan, 430071, China.

<sup>2</sup> School of Urban Construction, Wuchang University of Technology, Wuhan, 430223, China.

<sup>3</sup> Wuhan Municipal Construction Group Co., Ltd., Wuhan, 430023, China.

\* Corresponding Author: Chunguang Li. Email: cgli@whrsm.ac.cn.

Received: 07 November 2018; Accepted: 01 January 2019.

materials. Han et al. [Han and Chen (2014)] proposed a method for three-dimensional anisotropic slope stability based on the upper-bound limit analysis.

Many analytical methods and computer programs based on limit state analysis are available for analyzing the variation of undrained shear strength with direction. Up to now, however, very little work has been done on the effects of variation of internal friction angle with direction in cohesive-frictional materials. Partly because the variation of cohesion with direction is much more significant than the effects of anisotropy on friction angles, but mostly due to the fact that it is generally more difficult to deal with the variation of internal friction angle with direction.

Limit analysis is a rigorous and powerful solution method for the stability problems. This paper will mainly concentrate on the effects of anisotropic friction angle in stability analysis for cohesive-frictional materials using upper bound limit analysis. In the present paper, the Mohr-Coulomb yield criterion has been linearized in  $\sigma$ - $\tau$  space by directions from x-axis, with which the cohesion and friction coefficient vary. The numerical formulation of the upper bound theorem using the modified anisotropic yield is then developed. The computational results obtained from numerical solutions were compared with those available in literature.

## 2 Upper bound theorems of limit analysis

An upper bound to the plastic limit load of a structure can be obtained by using the kinematic theorem of limit analysis [Drucker (1953)].

Consider a rigid-plastic volume  $V$  with boundary  $\partial V = \partial_u V \cup \partial_t V$  and  $\varnothing = \partial_u V \cup \partial_t V$ . A body force  $\mathbf{b}$  acts on the volume of  $V$ . Displacements  $\bar{\mathbf{u}}$  are prescribed on  $\partial_u V$  and surface traction  $\bar{\mathbf{t}}$  on  $\partial_t V$ . Under these conditions, the upper bound theorem of limit analysis can be stated as follows:

The collapse will occur if and only if there exists a kinematically admissible velocity field  $\mathbf{u}$ , such that

$$W_{int} < W_{ext}, \quad (1)$$

where

$$W_{int} = \int_V \boldsymbol{\sigma}^T \dot{\boldsymbol{\varepsilon}} dV + \int_{\Gamma_D} \boldsymbol{\sigma}_n \Delta \dot{\mathbf{u}} dS \quad (2)$$

$$W_{ext} = \int_V \mathbf{b}^T \dot{\mathbf{u}} dV + \int_{\partial_t V} \bar{\mathbf{t}}^T \dot{\mathbf{u}} dS \quad (3)$$

$$\boldsymbol{\sigma} \in \{\boldsymbol{\sigma} | f(\boldsymbol{\sigma}) \leq 0\} \quad (4)$$

$$\boldsymbol{\varepsilon} = \frac{1}{2} (\nabla \mathbf{u} + \mathbf{u} \nabla) \quad (5)$$

$$\mathbf{u} = \bar{\mathbf{u}}, \text{ on } \partial_u V \quad (6)$$

in which  $\boldsymbol{\sigma}$  denotes the stress vector,  $\dot{\boldsymbol{\varepsilon}}$  denotes the plastic strain rate vector,  $\Gamma_D$  denotes the region in which a velocity field discontinuity occurs,  $\boldsymbol{\sigma}_n$  denotes the traction on  $\Gamma_D$ ,  $\Delta \dot{\mathbf{u}}$  denotes the velocity change across  $\Gamma_D$ ,  $f(\cdot)$  means yield criterion.

The Mohr-Coulomb yield criterion is one of the most widely used models in engineering practice. Under the plain strain condition, the Mohr-Coulomb yield criterion is stated as:

$$f = \sqrt{(\sigma_x - \sigma_y)^2 + (2\tau_{xy})^2} + (\sigma_x + \sigma_y) \sin \phi - 2c \cos \phi \leq 0 \quad (7)$$

where  $c$  and  $\phi$  are the cohesion and the internal friction angle of the material respectively.

### 3 Brief review of numerical upper limit analysis

To enforce the flow rule constraint at a finite number of points, three-node triangular elements with the unknown velocities as nodal variables are used by various authors [Sloan (1989); Yu and Sloan (1994); Krabbenhoft, Lyamin, Hjiatj et al. (2005)]. Fig. 1 shows the three-node triangular element for the upper bound formulation, in which velocities at each node are the unknowns. The velocities throughout each triangle can be represented a linear function according to

$$u = \sum_{i=1}^3 N_i u^i, \quad v = \sum_{i=1}^3 N_i v^i \quad (8)$$

where  $u^i$  and  $v^i$  are the nodal velocities in  $x$  and  $y$  directions and  $N_i$  are shape functions for the triangular element. These shape functions (also called interpolation functions) are

$$N_i = \frac{1}{2A} (a_i + b_i x + c_i y) \quad (9)$$

where

$$a_i = x_j y_k - x_k y_j, \quad b_i = y_j - y_k, \quad c_i = -x_j + x_k \quad (10)$$

$i, j, k$  are the three node indexes in counterclockwise order, respectively, and  $A$  is the area of the triangular element.

Using shape function, the strain rate in an element can be expressed as

$$\begin{cases} \dot{\epsilon}_x = \frac{\partial u}{\partial x} = \sum_{i=1}^3 b_i u^i \\ \dot{\epsilon}_y = \frac{\partial v}{\partial y} = \sum_{i=1}^3 c_i v^i \\ \dot{\gamma}_{xy} = \frac{\partial u}{\partial y} + \frac{\partial v}{\partial x} = \sum_{i=1}^3 (c_i u^i + b_i v^i) \end{cases} \quad (11)$$

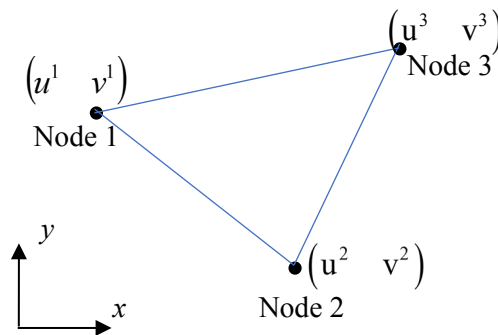


**Figure 1:** Three-node linear triangle element for upper bound limit analysis

#### 3.1 Flow rule constraints

According to the associated flow rule, the plastic strain can be established as follows:

$$\begin{cases} \dot{\epsilon}_x = \lambda \frac{\partial f}{\partial \sigma_x} \\ \dot{\epsilon}_y = \lambda \frac{\partial f}{\partial \sigma_y}, \lambda \geq 0 \\ \dot{\gamma}_{xy} = \lambda \frac{\partial f}{\partial \tau_{xy}} \end{cases} \quad (12)$$

where  $\lambda$  is described as the plastic multiplier and the superior dot denotes a derivative with respect to time.

To ensure that the formulation leads to a linear programming problem, the Mohr-Coulomb yield criterion in plane strain

$$f = \sqrt{(\sigma_x - \sigma_y)^2 + (2\tau_{xy})^2} + (\sigma_x + \sigma_y) \sin \phi - 2c \cos \phi \leq 0 \quad (13)$$

may be approximated by the following lines, as shown in Fig. 2

$$f_k = P_k \sigma_x + Q_k \sigma_y + R_k \tau_{xy} - 2c \cos \phi \leq 0, (k = 1, 2, \dots, p) \quad (14)$$

in which

$$\begin{cases} P_k = \cos \alpha_k + \sin \phi \\ Q_k = \sin \phi - \sin \alpha_k \\ R_k = 2 \sin \alpha_k \\ \alpha_k = 2\pi k/p \end{cases}$$

These define a polygon with  $p$  sides.

Substituting Eq. (14) to Eq. (12) gives

$$\begin{cases} \dot{\epsilon}_x = \sum_{k=1}^p \dot{\lambda}_k P_k \\ \dot{\epsilon}_y = \sum_{k=1}^p \dot{\lambda}_k Q_k, \dot{\lambda}_k \geq 0 \\ \dot{\gamma}_{xy} = \sum_{k=1}^p \dot{\lambda}_k R_k \end{cases} \quad (15)$$

Combining Eq. (11) and Eq. (15) leads to a set of equality constraints of the form

$$\begin{cases} \sum_{k=1}^p \dot{\lambda}_k P_k = \sum_{i=1}^3 b_i u^i \\ \sum_{k=1}^p \dot{\lambda}_k Q_k = \sum_{i=1}^3 c_i v^i \\ \sum_{k=1}^p \dot{\lambda}_k R_k = \sum_{i=1}^3 (c_i u^i + b_i v^i) \end{cases}, \dot{\lambda}_k \geq 0 \quad (16)$$

Thus, the nodal velocities and plastic multiplier rates for each triangular element are subject to three linear equality constraints and non-negativity constraints on each plastic multiplier rate.

### 3.2 Constraints in velocity discontinuities

According to the associated flow rule of Mohr-Coulomb yield criterion, the jumps in the tangential and normal velocities across a discontinuity have the following relationship

$$v_n = \tan \phi |u_t| \quad (17)$$

where

$$\begin{bmatrix} u_t \\ v_n \end{bmatrix} = \begin{bmatrix} \cos \theta & \sin \theta \\ -\sin \theta & \cos \theta \end{bmatrix} \begin{bmatrix} u_2 - u_1 \\ v_2 - v_1 \end{bmatrix}$$

and  $\theta$  is the inclination of the discontinuity boundary to the  $x$ -axis, shown in Fig. 3.

To remove the absolute value sign in Eq. (17), Sloan introduced two non-negative additional unknowns  $u_t^+$  and  $u_t^-$  [Sloan and Kleeman (1995)] such that

$$\begin{cases} u_t = u_t^+ - u_t^- \\ u_t^+ \geq 0 \\ u_t^- \geq 0 \end{cases} \quad (18)$$

Hence

$$|u_t| = u_t^+ + u_t^-$$

and the constraints in velocity discontinuities can be rewritten as

$$v_n = \tan \phi (u_t^+ + u_t^-) \quad (19)$$

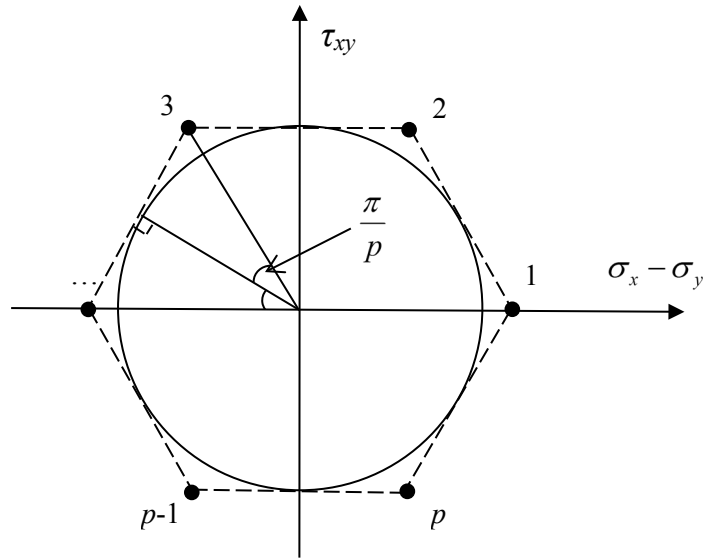


Figure 2: Linearization of Mohr–Coulomb yield function

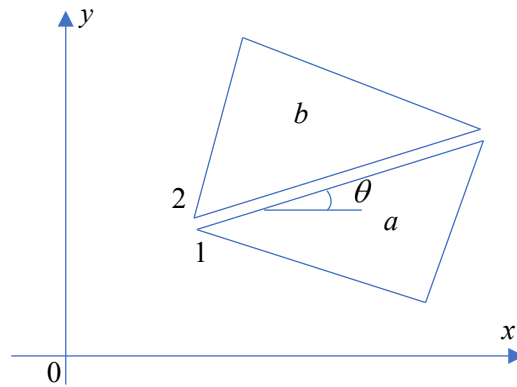


Figure 3: Velocity discontinuities on boundary of adjacent elements

### 3.3 Boundary conditions

According to upper bound theorem, the velocity field must satisfy the prescribed boundary conditions. For every node on the boundaries, the velocity must satisfy the following equality

$$\begin{bmatrix} \cos \theta & \sin \theta \\ -\sin \theta & \cos \theta \end{bmatrix} \begin{bmatrix} u \\ v \end{bmatrix} = \begin{bmatrix} \bar{u} \\ \bar{v} \end{bmatrix} \quad (20)$$

in which  $\theta$  is the angle between the outer normal vector of the boundary and the  $x$ -axis,  $\bar{u}$  and  $\bar{v}$  are the prescribed velocities in the  $x$  and  $y$  directions on the boundary.

### 3.4 Power dissipation

The power dissipated along a velocity discontinuous boundary is

$$P_d = \int_l c |u_t| dl = \sum_{k=1}^4 c_d^k u_k \quad (21)$$

and the power dissipated in an element is given by

$$P_c = \int_A (\sigma_x \dot{\epsilon}_x + \sigma_y \dot{\epsilon}_y + \tau_{xy} \dot{\gamma}_{xy}) dA$$

Substituting (11) and (14) into (22), we obtain

$$P_c = \sum_{k=1}^p c_c^k \dot{\lambda}_k \quad (22)$$

### 3.5 Linear programming problem

The constraint equations include flow rule constraints, velocity discontinuities constraints, and velocity boundary conditions. With those constraints the kinematic theorem may be expressed as a standard linear programming form

$$\text{Minimize: } (\mathbf{C}_c^T + \mathbf{C}_d^T) \mathbf{X} \text{ (Power dissipation),}$$

subject to:

$$(\mathbf{A}_1 - \mathbf{A}_2) \mathbf{X} = \mathbf{0} \text{ (Flow rule)}$$

$$\mathbf{A}_3 \mathbf{X} = \mathbf{0} \text{ (Velocity discontinuities constraints)}$$

$$\mathbf{A}_4 \mathbf{X} = \mathbf{B} \text{ (Velocity boundary conditions)}$$

$$\mathbf{X} \geq 0$$

where  $\mathbf{X}$  is a vector including nodal velocities and element plastic multiplier rates.

## 4 Linearization of the yield criterion in $\sigma$ - $\tau$ space and constraints for plastic flow

### 4.1 Linearization of the yield criterion in $\sigma$ - $\tau$ space

The Mohr-Coulomb yield criterion may be written as

$$|\tau| \leq c + f \sigma_n, \quad (23)$$

where  $c$  and  $f$  are cohesion and friction coefficient,  $\tau$  and  $\sigma_n$  are the shear and the normal stress on a plane with normal unit vector  $n = [\cos \alpha, \sin \alpha]^T$ , in which  $\alpha$  is the angle between the plane and the  $x$ -axis. The normal stress and the corresponding shear stress on the plane can be expressed as

$$\sigma_n = [\cos^2 \alpha \quad \sin^2 \alpha \quad \sin 2\alpha] \begin{bmatrix} \sigma_x \\ \sigma_y \\ \tau_{xy} \end{bmatrix}, \quad (24)$$

and

$$\tau = \begin{bmatrix} -\frac{1}{2}\sin 2\alpha & \frac{1}{2}\sin 2\alpha & \cos 2\alpha \end{bmatrix} \begin{bmatrix} \sigma_x \\ \sigma_y \\ \tau_{xy} \end{bmatrix}. \quad (25)$$

The Mohr's circle is approximated by an interior polygon with  $p$  vertices starting from  $(\sigma_x, \tau_{xy})$ , as shown in Fig. 4. The Mohr-Coulomb yield criterion can be discretized as

$$M_k \sigma_x + N_k \sigma_y + P_k \tau_{xy} \leq c_k; k=1,2,\dots,p \quad (26)$$

where

$$\begin{aligned} M_k &= -\frac{1}{2}\sin\left(\frac{2k\pi}{p}\right) - \cos^2\left(\frac{k\pi}{p}\right)f_k \\ N_k &= \frac{1}{2}\sin\left(\frac{2k\pi}{p}\right) - \sin^2\left(\frac{k\pi}{p}\right)f_k \\ P_k &= \cos\left(\frac{2k\pi}{p}\right) - \sin\left(\frac{k\pi}{p}\right)f_k \end{aligned} \quad (27)$$

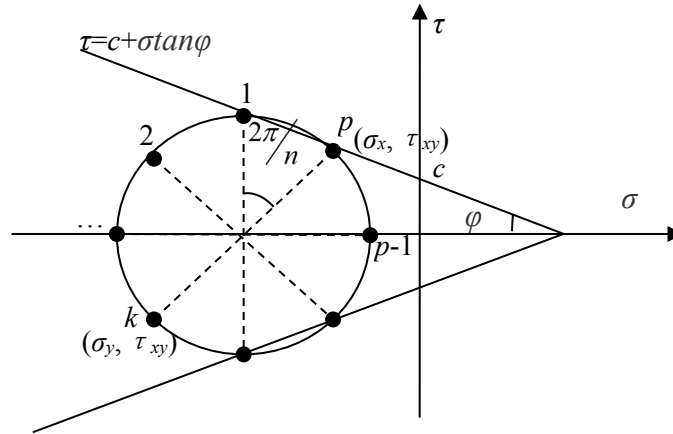


**Figure 4:** Discretization of Mohr's circle in  $\tau$ - $\sigma$  space

From Fig. 4, we can see that at least one point on the Mohr circle is on the yield surface. The same effect may be achieved as the external polygon is used to approach Mohr circle by traditional discretization method.

What's worth mentioning is that  $c$  and  $f$  in Eqs. (26) and (27) can vary with direction for anisotropic materials.

#### 4.2 constraints for plastic flow

Substituting Eq. (26) into Eq. (12), the plastic flow becomes

$$\begin{cases} \dot{\epsilon}_x = \sum_{i=1}^p \lambda_i M_i \\ \dot{\epsilon}_y = \sum_{i=1}^p \lambda_i N_i, \lambda \geq 0 \\ \dot{\gamma}_{xy} = \sum_{i=1}^p \lambda_i P_i \end{cases} \quad (28)$$

## 5 Anisotropy of soils

It is frequently the case that the shear strength of clay deposits exhibits some anisotropy with regard to direction [Al-Shamrani (2005)]. The failure criteria for anisotropic materials has been paid attention by many researchers [Bishop (1966); Chen, Snitbhan and Fang (1975); Reddy and Rao (1981)].

The cohesion strength  $c$  and the internal friction coefficient  $f$  can be given by

$$c = c(\theta) \quad (29)$$

$$f = f(\theta) \quad (30)$$

where  $\theta$  represents the angle between the horizontal direction and the direction of a plane where the cohesion  $c$  or the internal coefficient  $f$  is measured.

As shown diagrammatically in Fig. 5. The shear strength, taking cohesion strength  $c$  as an example, varies with direction in vertical-horizontal plane. The  $c_k$  and  $f_k$  in Eqs. (26) and (27) can be simply substituted by  $c(\theta_k)$  and  $f(\theta_k)$  in the direction  $\theta_k$  for anisotropic materials.

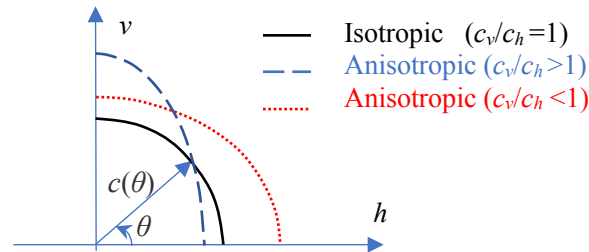


**Figure 5:** Variation of strength with direction in vertical-horizontal plane

## 6 Numerical examples

### 6.1 Example 1: Isotropic slope

This example is taken from Zheng et al. [Zheng, Tham and Liu (2006)]. The section of a slope including two kinds of soils is shown in Fig. 6, the mechanical parameters are listed in Tab. 1, and Fig. 7 illustrates the mesh and the boundary conditions.

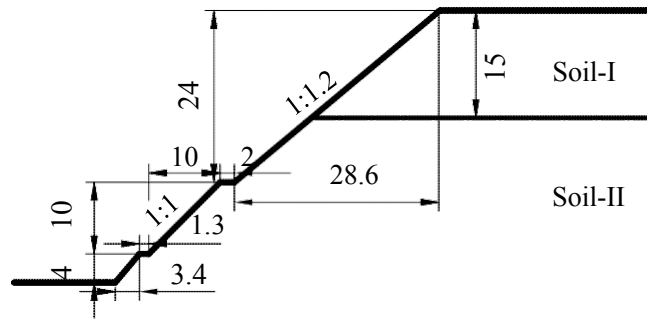
Fig. 8 illustrates the respective factors of safety obtained from upper bound analysis with different vertex point numbers, and the results converge to a stable solution from above as the vertex point number increases. When Vertex number  $p=28$  the factor of safety is 1.507, which is slightly larger than the Spencer's method 1.43 by 5%, but the difference will be smaller as the mesh is refined.

Fig. 9 shows the critical velocity field of the isotropic slope, which reflects the plastic collapse mode of the slope.

Similarly, with classical finite element method, the FOS acquired by the present method will also converge with the increasing of the element numbers, as is shown in Fig. 10.

**Table 1:** Parameters for soils in Example 1

| Soil    | $\gamma$ (kN/m <sup>3</sup> ) | $c$ (kPa) | $\phi$ (°) | $E$ (MPa) | $\nu$ |
|---------|-------------------------------|-----------|------------|-----------|-------|
| Soil-I  | 24.0                          | 34.0      | 26         | 2E4       | 0.35  |
| Soil-II | 25.0                          | 39.0      | 35         | 5E4       | 0.30  |



**Figure 6:** The slope section for Example 1

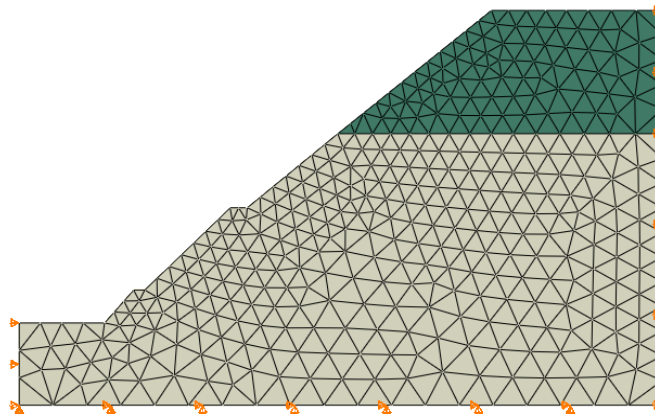


**Figure 7:** Meshes for Example 1

**Table 2:** Safety factors for different number of vertex points

| Vertex number $p$ | 4     | 8     | 12    | 16    | 20    | 24    | 28    | Spencer's Method |
|-------------------|-------|-------|-------|-------|-------|-------|-------|------------------|
| Factor of safety  | 1.668 | 1.555 | 1.524 | 1.516 | 1.511 | 1.509 | 1.507 | 1.43             |

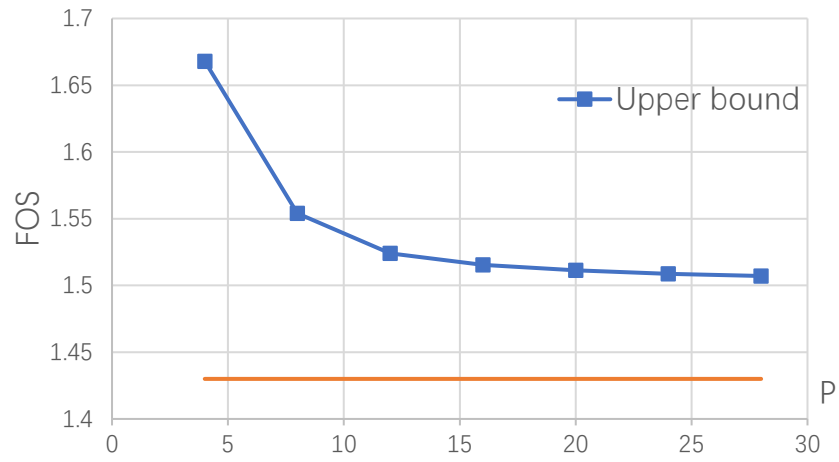


**Figure 8:** Relationships between factor of safety and vertex number  $p$

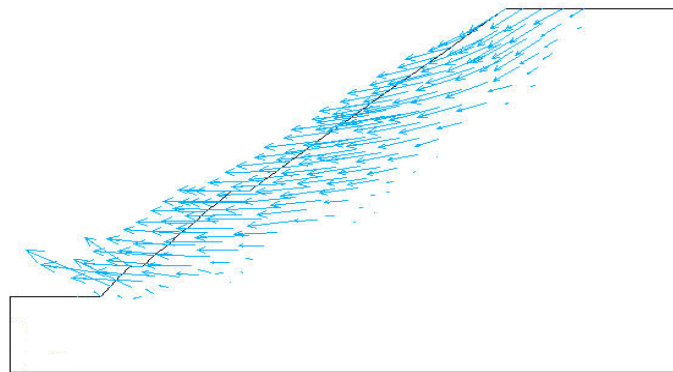


**Figure 9:** Critical velocity field of Example 1

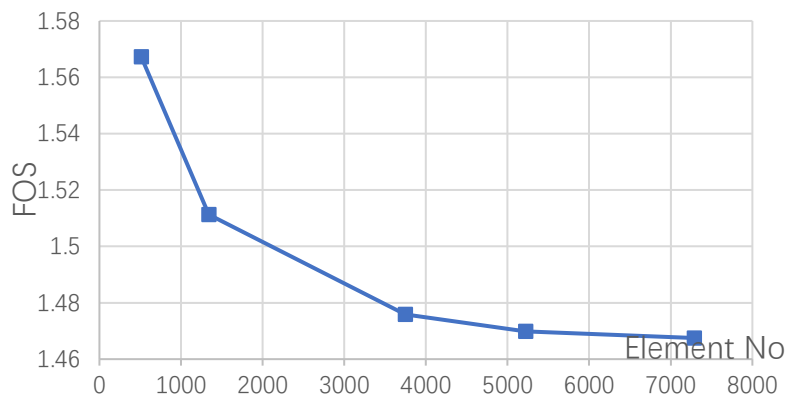


**Figure10:** FOS for different vs. element numbers

**Table 3:** Safety factors for different element numbers

| Element number   | 512    | 1341   | 3749   | 5221   | 7287   | Spencer's Method |
|------------------|--------|--------|--------|--------|--------|------------------|
| Factor of safety | 1.5673 | 1.5113 | 1.4759 | 1.4698 | 1.4675 | 1.43             |

### 6.1 Example 2: A trapdoor in anisotropic clay

This example is taken from Yu et al. [Yu and Sloan (1994)].

For anisotropic soils, based on the earlier studies [Casagrande and Carillo (1944); Lo (1966)], the cohesion,  $c$ , with the major principal stress inclined at an angle  $\theta$  with the horizontal may be written in the form:

$$c = c_h \cos^2 \theta + c_v \sin^2 \theta = c_h \left[ 1 + \left( \frac{c_v}{c_h} - 1 \right) \sin^2 \theta \right] \quad (31)$$

where  $c_h$  and  $c_v$ , are the cohesion strengths in the horizontal and vertical directions, respectively.

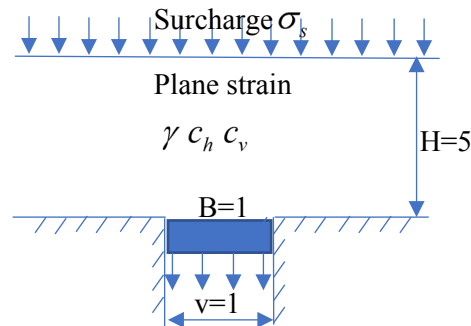
Fig. 11 shows the geometry of the example, and the mesh used to model a trapdoor with  $H/B=5$ . To compute the stability for a fixed  $H/B$  value, the surcharge and soil unit weight are set to zero [Yu and Sloan (1994)]. Due to symmetry, only one half of the geometry needs to be considered and the mesh is as shown in Fig. 12.

The stability factor for the trapdoor in isotropic clay is proven to be  $N=(\gamma H+\sigma_s-\sigma_t)/c_h$  [Sloan, Assadi and Purushothaman (1990)], where  $\gamma$  is the unit weight of the soil.

The upper bounds of stability for various ratios of  $c_v/c_h$ , using 24-vertex to discretize the yield criterion, are listed in Tab. 3 and shown in Fig. 13. Displacement contours for  $c_v/c_h=0, 1$  and 2 are shown in Fig. 14. It can be seen that the upper bounds agree well with that obtained by Yu's method when  $c_v/c_h \geq 1$ , especially, the presented method gives a more accurate upper bound than Yu's result when  $c_v/c_h < 1$ , and it is easy to see that the stability factor  $N$  should be 0 when  $c_v = 0$ , which is verified by the present numerical results, and the soil rests on a trapdoor would vertically slip down along the wall of the strap, as shown in Fig. 14 (a).

**Table 3:** Safety factor for trapdoor problem

| $c_v/c_h$        | 0 | 0.5   | 1     | 1.5   | 2     |
|------------------|---|-------|-------|-------|-------|
| Factor of safety | 0 | 3.685 | 6.354 | 7.038 | 7.608 |

**Figure11:** Trapdoor problem

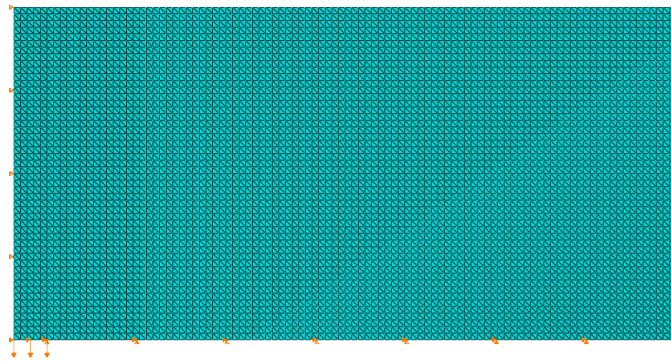


**Figure12:** Mesh used for analysis of the trapdoor problem (element size=0.1)

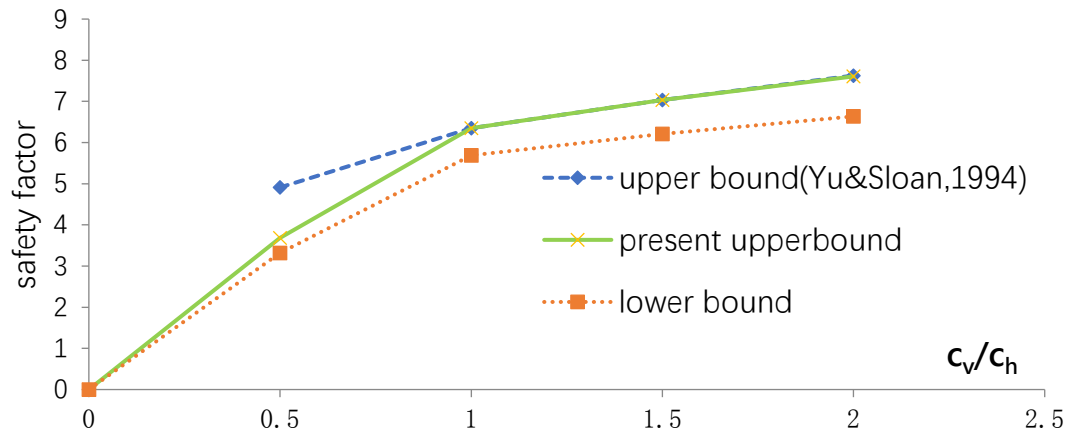
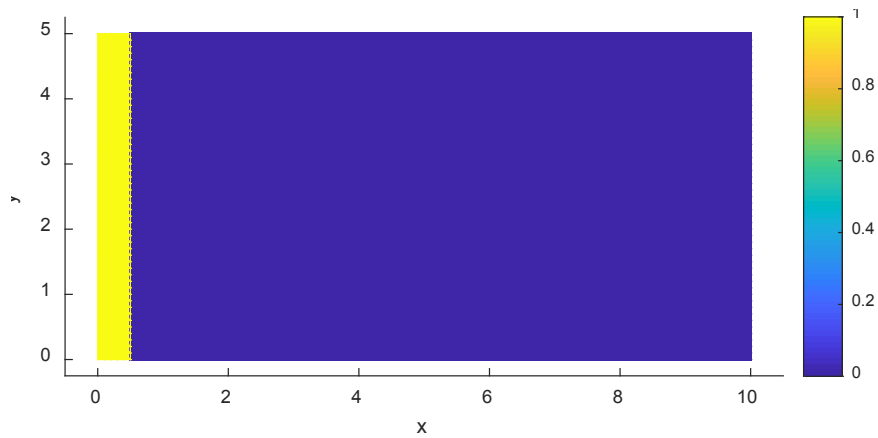


**Figure 13:** Stability factor against the value of  $c_v/c_h$



(a)  $c_v/c_h=0$

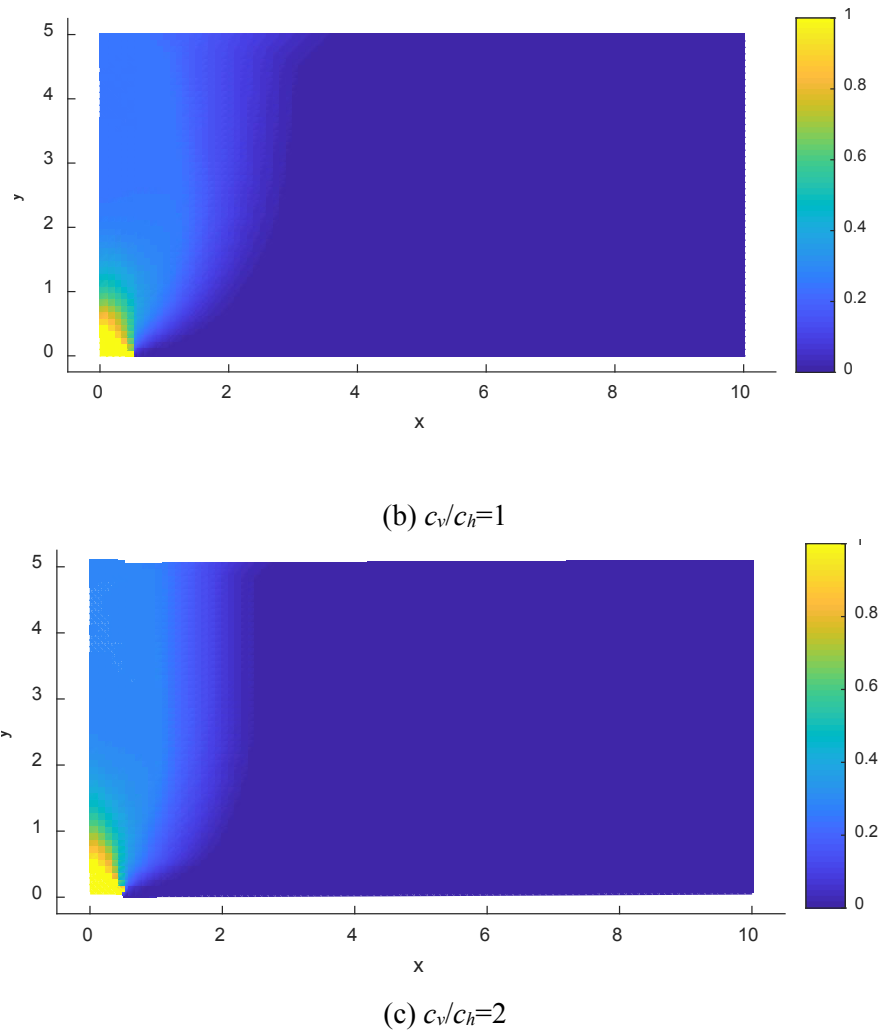


**Figure 14:** Contours of displacement at limit state for  $c_v/c_h = 0, 1$  and  $2$ , respectively

It is worth to note that although the upper bound limit analysis can provide a failure mode, there are some other methods which can give the failure mode, such as slip line method [Rabczuk and Areias (2006)]. Since the limit analysis deals with ideal elastic plastic materials, it cannot describe the crack propagation process [Rabczuk, Zi, Bordas et al. (2010)], especially for rock slope stabilities. However, the latest phase method can solve this complicated problem easily [Zhou, Rabczuk and Zhuang (2018); Zhou, Zhuang and Rabczuk (2018); Zhou, Zhuang, Zhu et al. (2018)].

The uncertainty is another important problems [Hamdia, Ghasemi, Zhuang et al. (2018)], which plays an important role in slope stabilities. It is especially encouraging that there a lot of off-the-shelf software can be used, for example, MATLAB toolbox [Vubac, Lahmer, Zhuang et al. (2016)].

## 7 Conclusions

To develop the upper bound numerical formulations for anisotropic soil, the Mohr's circle is discretized in  $\sigma$ - $\tau$  space, and then a general finite element formulation of the upper bound theorems is presented. The presented method is as simple and efficient as the traditional one, and the advantage of the present method is that it affords an approach to tackle the anisotropic materials whose cohesion and friction coefficient varies with direction. Two numerical examples given in the paper illustrate that the proposed numerical procedure can be used to compute rigorous upper bound solutions of anisotropic soils.

**Funding Statement:** The authors received no specific funding for this study.

**Conflicts of Interest:** The authors declare that they have no conflicts of interest to report regarding the present study.

## References

- Al-Karni, A. A.; Al-Shamrani, M. A.** (2000): Study of the effect of soil anisotropy on slope stability using method of slices. *Computers and Geotechnics*, vol. 26, no. 2, pp. 83-103.
- Al-Shamrani, M. A.** (2005): Upper-bound solutions for bearing capacity of strip footings over anisotropic nonhomogeneous clays. *Soils and Foundations*, vol. 45, no. 1, pp. 109-124.
- Bishop, A.** (1966): The strength of soils as engineering materials. *Geotechnique*, vol. 16, no. 2, pp. 91-130.
- Casagrande, A.; Carillo, N.** (1944): Shear failure of anisotropic materials. *Journal of Boston Society of Civil Engineers*, vol. 31, no. 4, pp. 74-81.
- Chen, W. F.; Snitbhan, N.; Fang, H. Y.** (1975): Stability of slopes in anisotropic, nonhomogeneous soils. *Canadian Geotechnical Journal*, vol. 12, no. 1, pp. 146-152.
- Drucker, D. C.** (1953). Coulomb friction, plasticity, and limit loads, Graduate Division Of Applied Mathematics, Brown University. pp. 1-16.
- Hamdia, K. M.; Ghasemi, H.; Zhuang, X.; Alajlan, N.; Rabczuk, T.** (2018): Sensitivity and uncertainty analysis for flexoelectric nanostructures. *Computer Methods in Applied Mechanics Engineering*, vol. 337, no. 8, pp. 95-109.
- Han, C. Y.; Chen, J. J.; Xia, X. H.; Wang, J. H.** (2014): Three-dimensional stability analysis of anisotropic and non-homogeneous slopes using limit analysis. *Journal of Central South University*, vol. 21, no. 3, pp. 1142-1147.
- Krabbenhoft, K.; Lyamin, A. V.; Hjiiaj, M.; Sloan, S. W.** (2005): A new discontinuous upper bound limit analysis formulation. *International Journal for Numerical Methods in Engineering*, vol. 63, no. 7, pp. 1069-1088.
- Lo, K.** (1966): Stability of slopes in anisotropic soils. *Journal of Soil Mechanics & Foundations Div*, vol. 92, no. Closure, pp. 77-82.
- Nian, T.; Chen, G.; Luan, M.; Yang, Q.; Zheng, D.** (2008): Limit analysis of the stability of slopes reinforced with piles against landslide in nonhomogeneous and anisotropic soils. *Canadian Geotechnical Journal*, vol. 45, no. 8, pp. 1092-1103.

- Rabczuk, T.; Areias, P.** (2006): A new approach for modelling slip lines in geological materials with cohesive models. *International Journal for Numerical Analytical Methods in Geomechanics*, vol. 30, no. 11, pp. 1159-1172.
- Rabczuk, T.; Zi, G.; Bordas, S.; Nguyenxuan, H.** (2010): A simple and robust three-dimensional cracking-particle method without enrichment. *Computer Methods in Applied Mechanics Engineering*, vol. 199, no. 37, pp. 2437-2455.
- Reddy, A.; Rao, K. N. V.** (1981): Bearing capacity of strip footing on anisotropic and nonhomogeneous clays. *Soils and Foundations*, vol. 21, no. 1, pp. 1-6.
- Reinicke, K.; Ralston, T.** (1977): Plastic limit analysis with an anisotropic, parabolic yield function. *International Journal of Rock Mechanics & Mining Sciences & Geomechanics Abstracts*, vol. 14, no. 3, pp. 147-162.
- Sloan, S.; Kleeman, P.** (1995): Upper bound limit analysis using discontinuous velocity fields. *Computer Methods in Applied Mechanics and Engineering*, vol. 127, no. 1-4, pp. 293-314.
- Sloan, S. W.** (1989): Upper bound limit analysis using finite-elements and linear-programming. *International Journal for Numerical and Analytical Methods in Geomechanics*, vol. 13, no. 3, pp. 263-282.
- Sloan, S. W.; Assadi, A.; Purushothaman, N.** (1990): Undrained stability of a trapdoor. *Geotechnique*, vol. 40, no. 1, pp. 45-62.
- Vubac, N.; Lahmer, T.; Zhuang, X.; Nguyenthoi, T.; Rabczuk, T.** (2016): A software framework for probabilistic sensitivity analysis for computationally expensive models. *Advances in Engineering Software*, vol. 100, no. pp. 19-31.
- Yu, H.; Sloan, S.** (1994): Limit analysis of anisotropic soils using finite elements and linear programming. *Mechanics Research Communications*, vol. 21, no. 6, pp. 545-554.
- Yu, H.; Sloan, S.** (1994): Upper-bound limit analysis of a rigid-plastic body with frictional interfaces. *International Journal of Mechanical Sciences*, vol. 36, no. 3, pp. 219-229.
- Zheng, H.; Tham, L.; Liu, D.** (2006): On two definitions of the factor of safety commonly used in the finite element slope stability analysis. *Computers and Geotechnics*, vol. 33, no. 3, pp. 188-195.
- Zhou, S.; Rabczuk, T.; Zhuang, X.** (2018): Phase field modeling of quasi-static and dynamic crack propagation: COMSOL implementation and case studies. *Advances in Engineering Software*, vol. 122, no. 8, pp. 31-49.
- Zhou, S.; Zhuang, X.; Rabczuk, T.** (2018): A phase-field modeling approach of fracture propagation in poroelastic media. *Engineering Geology*, vol. 240, pp. 189-203.
- Zhou, S.; Zhuang, X.; Zhu, H.; Rabczuk, T.** (2018): Phase field modelling of crack propagation, branching and coalescence in rocks. *Theoretical Applied Fracture Mechanics*, vol. 96, pp. 174-192.